Estuarine, Coastal and Shelf Science 282 (2023) 108230

Contents lists available at ScienceDirect

Estuarine, Coastal and Shelf Science

journal homepage: www.elsevier.com/locate/ecss

A multiscale ocean modelling system for the central Arabian/Persian Gulf: From regional to structure scale circulation patterns

Emmanuel Hanert [a,b,*], Aboobacker Valliyil Mohammed [c], Subramanian Veerasingam [c], Thomas Dobbelaere [a], Valentin Vallaeys [a], Ponnumony Vethamony [c]

[a] Earth and Life Institute (ELI), UCLouvain, Louvain-la-Neuve, Belgium
[b] Institute of Mechanics, Materials and Civil Engineering (IMMC), UCLouvain, Louvain-la-Neuve, Belgium
[c] Environmental Science Center, Qatar University, Doha, Qatar

ARTICLE INFO

Keywords:
Unstructured-mesh ocean model
Qatar waters
Coastal eddies
Artificial structures
Ocean sprawl

ABSTRACT

The Arabian/Persian Gulf (hereafter, the "Gulf") is one the busiest and fastest changing sea in the World. Its circulation is primarily driven by the surface water inflow from the Sea of Oman and density-driven and wind-driven flows within the Gulf. The regional circulation in its central part, particularly around Qatar, could not be explored because of unavailability of measured current data and the coarse resolution opted for the entire Gulf modelling. In the present study, we developed a high-resolution ocean modelling system of the entire Gulf with a particular focus on Qatar coastal waters. The model uses an unstructured mesh with different resolutions ranging from ~5 km in the open ocean to ~150 m along the coast of Qatar and less than 40 m around artificial structures. The model results have been validated with in situ data collected off Qatar. It allows seamless simulations of hydrodynamic processes from the entire basin scale down to the scale of coastal structures. The study identifies seasonal variability in currents and eddies in the central part of the Gulf. It also suggests the existence of four prominent anticyclonic eddies in the Gulf of Salwa, south of Bahrain. At the structure scale, the flow is mostly tidally driven and can be intensified beyond 1 m/s through narrow passages such as between breakwaters or within artificial waterways. By explicitly representing the effect of ocean sprawl on the coastal circulation, our model has the potential to greatly improve the environmental impact assessment of coastal developments in the Gulf area.

1. Introduction

Over the last 20 years, the Arabian/Persian Gulf (hereafter referred to as the "Gulf") has experienced a rapid development, driven by the oil and gas boom. It resulted in massive coastal modifications to build artificial islands, waterfronts, causeways and ports (Martín-Antón et al., 2016). These developments were executed through land reclamation combined with dredging and construction activities. Besides resulting in marine habitat loss that severely impacted coral reefs, seagrass meadows and mangroves (Burt, 2014), they also had non-local effects as they modified the ocean circulation patterns. Such changes to the dynamics of currents and waves influence the transport of sediments, biological material and energy between separated areas within the seascape (Bishop et al., 2017). These processes will result in sediment volume to increase upstream of the structures and decrease downstream, modifications to larval connectivity pathways and changes to water residence time (Sheppard et al., 2010).

The Gulf ocean dynamics is reflected by its unique topographic and climatic conditions. Two-layer ocean circulation, i.e., wind and density driven, prevails in the Gulf with the formation of eddies in response to changes in wind patterns and density gradients between the Gulf and the Arabian Sea (Al Azhar et al., 2016; Hosseinibalam et al., 2011; J. and Sadrinasab, 2005). The currents induced by the northerly winds including Shamal winds in the Gulf are predominantly towards south/southeast. The higher rate of evaporation coupled with lower sea surface temperature (especially in winter) towards the head of the Gulf, increases the density contrast (Swift and Bower, 2003). The resulting horizontal pressure gradient generates a surface inflow of less denser water through the Strait of Hormuz and a denser outflow in the opposite direction. That is, the density driven inflow of the Indian Ocean Surface Water (IOSW) propagates along the Iranian coast as Iranian coastal current (ICC), which outflows from the northern Gulf through the Arabian coast to the Sea of Oman as dense bottom currents, thereby exhibits a reverse estuarine circulation (Chao et al.,

* Correspondence to: Croix du Sud 2 box L7.05.16 - 1348 Louvain-la-Neuve, Belgium.
E-mail address: emmanuel.hanert@uclouvain.be (E. Hanert).

https://doi.org/10.1016/j.ecss.2023.108230
Received 11 November 2021; Received in revised form 30 November 2022; Accepted 20 January 2023
Available online 21 January 2023

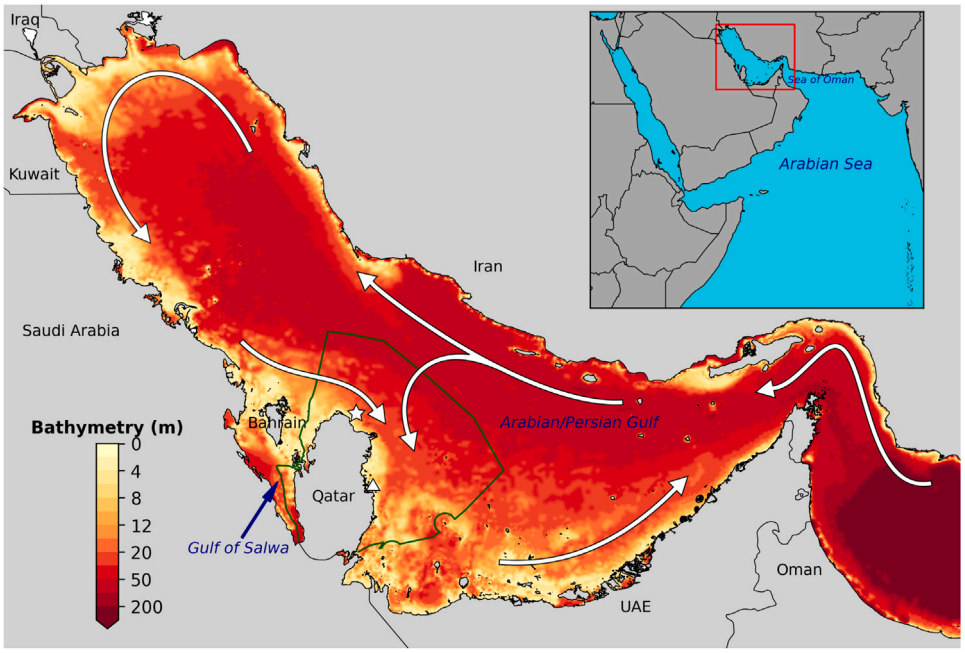

Fig. 1. Bathymetry of the Gulf with Qatar EEZ (green line). The bathymetry of Qatar waters is very shallow, with most of it shallower than 20 m. The locations where measurements were collected are represented by white "⋆" (Fuwairit) and "▲" (Doha Bay) symbols. Predominant surface circulation patterns are shown with white arrows. (For interpretation of the references to colour in this figure legend, the reader is referred to the web version of this article.)

1992; Reynolds, 1993; Johns et al., 2003; Hunter, 1983). The inflow is strong in summer and appears to reach as far as the northern end of the Gulf, because of the effect of southwest monsoon (see predominant circulation patterns in Fig. 1).

Variability of atmospheric and oceanographic forcing influences the circulations in the Gulf. For instance, evaporation leads to the formation of dense waters, which sink and flow towards the Sea of Oman through the Strait of Hormuz (Alosairi and Pokavanich, 2017; Hunter, 1982). A few studies have been carried out recently to understand the role of circulations and eddies in the Gulf, especially in the northern and central parts of the Gulf, which influence the physical and biogeochemical characteristics in the Gulf. Al Senafi and Anis (2020) identified significant changes in temperature and salinity in the northwestern Gulf during winter by the effect of wind driven circulation. Al-Ansari et al. (2015) reported that the hypoxia in the Gulf is due to two counterclockwise eddies in the northern and southern Gulf, developed by geographical settings of the Qatar Peninsula. The southward flowing density current along the eastern coast enables a strong thermocline at a depth of around 25 m during winter, at which the chlorophyll-a concentration is the maximum within the water column. It also develops a vertically homogeneous structure of dissolved oxygen in the offshore of Qatar during winter (Rakib et al., 2021). During summer, the denser southwestward flowing water mass sinks as the relatively fresher IOSW inflow enhances and thus forms stratified layers of water column in the central Gulf, especially in the Qatar waters (Elobaid et al., 2021).

While the mechanisms driving the baroclinic circulation and eddies in the Gulf are well known, the finer-scale details of the coastal circulation remain more elusive. Rakib et al. (2021) found that productivity in the Exclusive Economic Zone (EEZ) of Qatar has direct links with the Gulf circulation and eddies. In coastal regions, where depths are less than 25 m, the major controlling factors for coastal dynamics are wind and tide rather than the density driven circulation. However, a basin-scale eddy can induce small-scale eddies in conjunction with the coastal dynamics. The bathymetry and coastline features play a major role in modifying the circulation and formation of coastal eddies or tidal eddies. This was observed in the Gulf of Kachchh, located on the eastern arm of the Arabian Sea in the north (Vethamony et al., 2005). However, such features are not fully known or studied within the EEZ of Qatar. The current measurements in the EEZ of Qatar are very much limited to establish the circulation features or characterization of eddies.

Along the coast, the circulation is directly influenced by natural and artificial structures. The former includes mangrove forests, coral reefs and seagrass meadows, which are particularly abundant along the coast of Qatar (Butler et al., 2020). The latter includes numerous man-made structures protruding to the sea from the coast. In Qatar, these include the Pearl Project, Lusail City, the port of Doha, the industrial port of Mesaieed, the LNG terminal of Ras Laffan and the port of Al Ruwais (see locations in Fig. 2). The proliferation of these coastal artificial structures is part of a global ocean sprawl that is particularly important in the Gulf (Firth et al., 2016; Heery et al., 2017). The roughness and resistance induced by these structures changes the circulation along the coast. Changes in current direction and speed near the structures subsequently impact sediment transport, leading to changes in sediment accumulation and erosion rates, as well as changes to the transport patterns of drifting objects and substances. The downstream effect of artificial structures remains poorly understood and needs to be quantified to fully understand the effect of ocean sprawl on the marine environment (Heery et al., 2017).

Acquiring in-situ observations from a number of locations on a long-term basis is often difficult due to geographical and practical constraints. Well-proven fine resolution two-dimensional models are adequate to accurately simulate the coastal hydrodynamics, driven by winds and tides. Literature review suggests that no well-established numerical modelling study pertaining to the circulations in the EEZ of Qatar has been performed. For example, the numerical modelling studies along the northeastern coast of Qatar (Yousif, 2016; Yousif et al., 2018) describe only the circulation and sediment dispersion in a localized environment. In addition, spatial variability in currents over eco-sensitive areas such as coral reefs, seagrass meadows and mangrove forests of the Gulf are not well parametrized so far. Thus, it is important to have a predictive system across the EEZ of Qatar (i) to characterize the regional-scale circulation and its interactions with the topography and (ii) to quantify the small-scale hydrodynamic effects of the flow around coastal structures. The present study aims at developing a hydrodynamic modelling system that can bridge the

gap between the regional and structure scales in order to seamlessly represent the complex ocean circulation patterns in the central part of the Gulf.

2. Data and methods

2.1. Study area

The Gulf is a semi-enclosed, hypersaline and shallow ocean basin connecting the Indian Ocean through the Strait of Hormuz and Sea of Oman. The Strait of Hormuz is around 56 km wide. The water depths in the Gulf are generally shallow, with a maximum depth of 90 m and average depth of around 35 m (Barth and Khan, 2008). Complex bathymetry with numerous small and big islands, coral reefs, seagrass meadows, mangrove forests, mud and sand flats are the peculiar topographic features of the Gulf (Khan et al., 2002). Extreme hot summer, moderate cold winter, Shamal winds, dust storms, high evaporation and weak precipitation are the dominant climatic features. The major winds in the Gulf are northerlies and northwesterlies, with dominant contribution of Shamal winds (Al Senafi and Anis, 2015; Yu et al., 2016). The intensity and duration of Shamal winds are higher during winter than in summer. In winter, the Shamal winds transport cold and dry air that enhances surface heat loss and evaporation, leading to the formation of high saline and cold water in the Gulf (Thoppil and Hogan, 2010). Although the occurrence is relatively low, the easterly Nashi winds and the southeasterly Kaus winds are also blown over the Gulf in higher magnitudes (Aboobacker et al., 2021a).

The EEZ of Qatar lies in the central part of the Gulf, which extends from the coast to offshore territory bounded by the territorial waters of Saudi Arabia, Bahrain, Iran and United Arab Emirates. The water depths are generally shallow (less than 20 m), except in a few regions, where the maximum depth is around 70 m (Fig. 1). Shamal winds persist over Qatar during summer and winter with relatively high occurrence during winter (Rao et al., 2003). In addition, sea–land breezes also occur in definite proportion throughout the year (Sandeepan et al., 2018; Eager et al., 2008). The sea surface temperature is around 18–22 °C during winter (Belthaji, 1983) and around 31–36 °C during summer (Riegl and Purkis, 2012). The salinity of Qatar waters is generally between 39 and 46 (Rakib et al., 2021; Al-Ansari et al., 2015). It can however exceed 60 in regions like the Gulf of Salwa (GoS) (Joydas et al., 2015) and reach around 70–80 in tidal pools and lagoons, which are the extreme environmental tolerance limits of marine organisms in the Gulf (Price et al., 1993).

2.2. In-situ measurements

Publicly-available long-term in situ measurements (such as tides, currents and waves) are very limited in the Gulf area and in particular in Qatar EEZ. Private companies often collect information for specific projects but these are primarily classified in nature. For this study, we measured sea surface elevation (SSE) and currents' velocity at two nearshore locations: offshore of Fuwairit on the northeast coast of Qatar (26.123733 N, 51.373283 E) and in Doha Bay (25.328733 N, 51.564366 E) to validate the hydrodynamic model results (see locations of in Fig. 1). Offshore of Fuwairit, both the current velocity and SSE were measured every 10 min between October 29th and November 26th 2019. In Doha Bay, only the SSE was measured every 10 min between December 8th 2021 and January 17th 2022. Measurements were taken with a Seaguard Recording Current Meter (RCM) fitted with wave and tide sensors. The mean accuracy of the RCM Doppler Current Sensor (DCS) is 0.15 cm/s for the current velocity over a range of 0–300 cm/s and ±5° for the current direction within 0–360° (Victoria, 2011). The RCM wave and tide sensors have an accuracy of ±0.02% Full Scale Output (FSO).

2.3. Hydrodynamic model

We simulate the ocean circulations in the Gulf with the multi-scale ocean model SLIM.[1] SLIM solves the ocean circulation governing equations with the Discontinuous Galerkin finite element method on an unstructured mesh. The mesh resolution can thus be varied in space. It can be increased where small-scale flow features are thought to be important while keeping it coarser in more uniform areas. Computational resources can therefore be directed where they are most needed. SLIM can be used in a wide range of situations since it consists of a 1D river model, a 2D depth-averaged model and a 3D baroclinic model. It has already been successfully applied to several complex coastal environments around the world such as the Great Barrier Reef (Legrand et al., 2006; Lambrechts et al., 2008; Thomas et al., 2014), the Florida Reef Tract (Frys et al., 2020; Dobbelaere et al., 2020), the Mahakam river delta (de Brye et al., 2011) and the Congo river-to-sea system (Le Bars et al., 2016; Vallaeys et al., 2021).

In this study we use SLIM2D, the depth-averaged version of SLIM, that solves the non-linear shallow water equations:

$$\frac{\partial \eta}{\partial t} + \nabla \cdot (H\mathbf{u}) = 0, \tag{1}$$

$$\frac{\partial \mathbf{u}}{\partial t} + \mathbf{u}\cdot\nabla\mathbf{u} + f\mathbf{e}_z \times \mathbf{u} = -g\nabla\eta - \frac{g}{H}\int_{-h}^{\eta} \nabla\left[\int_z^{\eta} \frac{\rho-\rho_0}{\rho_0}\, \mathrm{d}z'\right] \mathrm{d}z + \mathbf{F} + \mathbf{D}, \tag{2}$$

where η is the SSE, $H = h + \eta$ is the water column height, h is the bathymetry, $\mathbf{u}$ is the depth-integrated velocity, f is the Coriolis factor, $\mathbf{e}_z$ is a unit vector pointing vertically upwards, g is the gravitational acceleration, ρ is the three-dimensional water density, $\rho_0 = 1027\ \mathrm{kg/m^3}$ is a reference density value, $\mathbf{F}$ includes all the regional external forcings and $\mathbf{D}$ includes all the momentum dissipation terms. The bathymetry h is extracted from the GEBCO 2019 global terrain model with a 15 arc-second resolution (Becker et al., 2009). When the bathymetry data is read into the hydrodynamic model, the minimum depth is set to $h = 2$ m in order to be sure that the entire domain is under water at all time. While GEBCO is probably the most accurate open-source bathymetry dataset, its reliability might be suboptimal around artificial structures because of frequent dredging and more intense sediment erosion and deposition. The precise depth at which port access channels are dredged is generally not publicly-available. Eqs. (1)–(2) are solved with free-slip boundary conditions on the coastline and with Flather boundary conditions on the open boundary, in the Sea of Oman. Flather boundary conditions amount to impose a combination of the SSE and the current velocity to prescribe the incoming characteristic variable (also called Riemann invariant, Blayo and Debreu, 2005). The velocity imposed on the open boundary is the sum of the depth-averaged velocity provided by the Mercator global ocean analysis produced by running the global data-assimilated ocean model NEMO on a $1/12°$ grid (Ferry et al., 2007), and the tidal velocity obtained from the OSU TPXO9-atlas dataset (computed on a $1/30°$ grid in the Gulf, Egbert et al., 2002). The SSE imposed on the open boundary is computed in the same way. The model equations are initialized with zero SSE and velocity fields and we consider a one week spin-up period.

Unlike previous applications of SLIM2D, in this study we have taken into account the horizontal baroclinic pressure gradient. This term is usually neglected in 2D coastal models as the atmospheric and astronomical forcings are often the main drivers of the circulation. However, in the Gulf, the evaporation is so large that salinity can become very large (up to 70–80), hence leading to non-negligible horizontal density gradients. The usual approach to represent density effects is to use a 3D baroclinic model that explicitly represents the salinity and temperature evolution. Doing so however strongly increases the computational

[1] SLIM: Second-generation Louvain-la-Neuve Ice-ocean Model, www.slim-ocean.be.

cost and hence requires to sacrifice the horizontal resolution. Here, we consider a different approach by passing the baroclinic information computed by a large-scale 3D baroclinic model to SLIM2D. This amounts to force SLIM2D with the internal mode of another model. The density ρ is computed from the salinity and temperature fields of the same Mercator global ocean analysis as the one used to force the velocity and SSE on the open boundary.

The external forcings are expressed as follows:

$$\mathbf{F} = \frac{\boldsymbol{\tau}}{\rho_0 H} + \gamma \left(\mathbf{u}_\star - \mathbf{u}\right). \tag{3}$$

The first forcing depends on the surface wind stress:

$$\boldsymbol{\tau} = \rho_{air} C_w \|\mathbf{u}_{10}\| \mathbf{u}_{10}, \tag{4}$$

where, ρ_{air} is the air density, C_w is the wind drag coefficient and $\mathbf{u}_{10}$ is the wind speed (in ms^{-1}) at 10 m above the sea surface (Cushman-Roisin and Beckers, 2011). The wind speeds are taken from the European Centre for Medium-Range Weather Forecasts (ECMWF) ERA5 reanalysis. ERA5 has a spatial resolution of 31 km and a temporal resolution of 1 h. The performance of ERA5 surface winds was tested globally by comparing with Advanced Scatterometer (ASCAT) winds (Belmonte Rivas and Stoffelen, 2019). The comparison of ERA5 wind speed and direction with measurements in the Gulf resulted in a correlation coefficient of 0.95 and 0.93 and bias of 0.07 m/s and 4.3°, respectively (Mahmoodi et al., 2019). Recently, Aboobacker et al. (2021c) validated the ERA5 winds, specific to the Qatar coast. The drag coefficient is computed using the (Smith and Banke, 1975) parametrization to take into account the fact that stronger winds cause rougher sea surface and therefore increase the value of C_w:

$$C_w = 0.001(\alpha + \beta \|\mathbf{u}_{10}\|), \tag{5}$$

where, $\alpha = 0.63$ and $\beta = 0.066$ s/m. With this parametrization, the wind drag coefficient does not saturate for large wind speeds. It is therefore not suitable for storm conditions when the wind is strong enough to blow off white cap from the crest of the waves, hence generating a layer of droplets that acts as a slip layer for the winds at the ocean-atmosphere interface. The (Smith and Banke, 1975) parametrization used here is hence only valid for wind speeds less than about 20 m/s, which is generally the case in the Gulf.

The second forcing is a flow relaxation term, and its goal is to keep the model velocity close to real currents $\mathbf{u}_\star$ in deep areas, where the flow cannot be approximated by a 2D model. In this study, we have expressed $\mathbf{u}_\star$ as the same combination of the depth-averaged Mercator velocity and the OSU TPXO tidal velocity as the one used for the open boundary condition. The coefficient γ controls the importance of the relaxation term. It vanishes in shallow areas, where the flow is mostly 2D and plays a role only in deep areas, where 3D processes cannot be neglected. Here, we have chosen to set γ to 0 for depths shallower than 50 m. Elsewhere, the value of γ increases linearly with the water depth beginning with a value of 5×10^{-6} s^{-1} at 50 m depth and raising up to a maximum value of 3×10^{-5} s^{-1} at 300 m depth and beyond. As a result, this flow relaxation term plays a role mostly in the Sea of Oman, near the open boundary.

Finally, the momentum dissipation is expressed as follows:

$$\mathbf{D} = \frac{1}{H}\boldsymbol{\nabla} \cdot [H\nu(\boldsymbol{\nabla}\mathbf{u})] - \frac{C_d \|\mathbf{u}\| \mathbf{u}}{H}. \tag{6}$$

The first term is the usual momentum diffusion with a (Smagorinsky, 1963) non-linear horizontal viscosity ν. The second term is a quadratic bottom drag, characterized by a bulk drag coefficient C_d. In this study, we take for C_d the canonical value of 0.0025 found for muddy or sandy sea beds, except over coral reefs, where it is increased by a factor of 10 (Monismith, 2007). This is a rather simple parametrization of coral reefs bottom drag as it depends on several factors such as the reef three-dimensional geometry and its depth (Lentz et al., 2017). Since the objective of this study is not to look at the details of the flow over coral reefs, the simple parametrization is deemed sufficient. The reefs location is taken from UNEP-WCMC (2021).

The model accuracy directly depends on the resolution of the underlying mesh on which the model equations are solved. An unstructured mesh allows us to vary the resolution in space, and hence concentrate computational resources where they are most needed. Here, we use a mesh with a resolution of ~600 m along the coastline of all the countries surrounding the Gulf and the Sea of Oman. The same resolution is also used over coral reefs and around islands inside the Gulf. Far away from the coast, the resolution is reduced to ~5 km. The mesh resolution is increased by a factor of 4 (hence reaching ~150 m) along the coast of Qatar. This allows us to explicitly represent intricate natural features such the inland sea of Khor al Adaid in southeast Qatar. The mesh resolution is further increased by a factor of 4 (hence reaching ~37.5 m) around some man-made structures of interest such as the coastline of Doha (including the Pearl, Lusail and the port of Doha), the ports of Mesaieed, Al Ruwais and Ras Laffan. The latter is the world's biggest petrochemical export port with the world's largest LNG export facility (see Fig. 2). The finest mesh resolution is required to resolve topographically-driven flow features near artificial structures. Changing the mesh resolution and refinement criteria is straightforward, which makes this present model very flexible and easy to adapt to the application being considered. The mesh has been generated with the open-source mesh generator GMSH (Geuzaine and Remacle, 2009). It has about 8×10^5 elements.

3. Results and discussions

In this section, we first present the velocity measurements that were collected for this study. We then use these measurements to validate the model described in the previous section. The model is subsequently applied to investigate the seasonal variability of the basin-scale circulation and the structure-scale flow patterns.

3.1. Measured currents off Fuwairit

Velocity measurements indicate that the currents off Fuwairit follow the spring–neap cycle according to the tidal periodicity (Fig. 3a). In addition, diurnal variability in current speed is observed as a combination of ebb–flood patterns as well as diurnal variability in the wind speed and direction. Current speeds exceeding 0.4 m/s were recorded during the measurement period; the mean current speed was 0.19 m/s and the standard deviation 0.11 m/s. The predominant current direction is southeast or northwest, being tide-dominated; however, the effects of northerly/northwesterly Shamal winds and easterly winds are often visible. For instance, the northwest component of the currents was almost nullified by a strong Shamal wind event during 19–22 Nov 2019, when the currents were southeast. On the other hand, the strong easterly winds occurred during 10–11 Nov 2019 enhanced the northwest flow. The concurrent wave measurements carried out in this location indicate similar variations associated with Shamal and easterly winds (Aboobacker et al., 2021a).

3.2. Hydrodynamic model validation

Model results have been validated against currents velocity and SSE measurements off Fuwairit and in Doha Bay (see location in Fig. 1). We considered separate model runs for each of the two observation periods (see details in Section 2.2). Off Fuwairit, the model current speed and direction matched well with the observations (Fig. 3). The model correctly captured the prevailing northwest-to-southeast current dynamics, with velocity peaks exceeding 0.4 m/s. It also reproduced the strong Shamal wind event that occurred during 19–22 November. Being relatively strong, these Shamal-driven currents prevented the tidal currents from developing towards the northwest direction. Although the model has reasonably predicted the currents, current speeds were

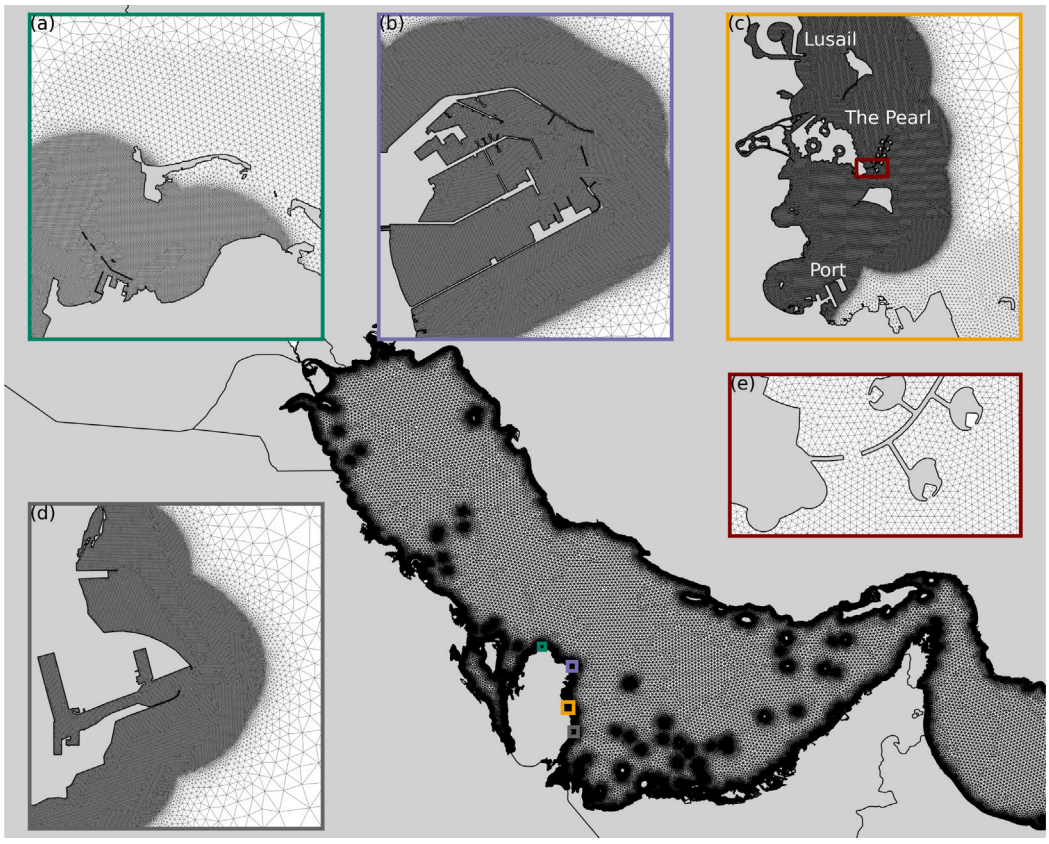

Fig. 2. The model mesh has a minimal coastal resolution of ~600 m, which is refined to ~150 m along the coast of Qatar, and further refined less than 40 m around artificial structures such as (a) the port of Al Ruwais, (b) the LNG terminal of Ras Laffan, (c) the coastline of Doha, (d) the industrial port of Mesaieed, and (e) the narrow passages within The Pearl, in Doha.

Table 1
Tidal current ellipse parameters for current meter observations and modelled currents. The parameters include the semi-major axis (L_{maj}), the semi-minor axis (L_{min}), the orientation angle (θ) and the phase (g).

Tidal	L_{maj} (cm/s)		L_{maj} (cm/s)		θ (degrees)		g (degrees)	
component	Obs.	Mod.	Obs.	Mod.	Obs.	Mod.	Obs.	Mod.
K1	19.53	15.34	0.18	0.59	128.08	133.00	95.41	94.85
M2	16.57	16.56	0.10	1.54	141.33	145.78	315.69	340.28
S2	9.31	7.05	0.10	0.55	143.44	142.50	339.62	1.56
O1	8.43	6.50	0.30	0.25	129.96	137.56	61.34	67.85
MSF	5.13	4.84	0.47	0.10	139.13	131.23	43.92	40.13
N2	2.57	3.04	0.15	0.51	148.25	147.41	269.06	316.31

sometimes under or overestimated, which could be attributed to the coarse spatial resolution of winds as well as possible inconsistencies in the GEBCO bathymetry near the coast. Over the entire timeseries, the root mean square error (RMSE) on the hourly current speed values is 10.8 cm/s and the mean absolute error (MAE) is 8.5 cm/s. The model SSE also compares very well with observations both off Fuwairit and in Doha Bay (Fig. 4). At both locations, the model correctly reproduces the spring–neap tidal cycle. The RMSE (resp. MAE) on the SSE is 9.8 cm (resp. 8.1 cm) off Fuwairit and 8.2 cm (resp. 6.7 cm) in Doha Bay.

A more detailed validation of the current velocity off Fuwairit is achieved by computing the tidal current ellipse parameters for both observed and simulated currents. These parameters were computed using the UTide packages (Codiga, 2011). They include the semi-major axis (L_{maj}), semi-minor axis (L_{min}), the orientation angle of semi-major axis (θ, counterclockwise from the east), and phase (g). We have considered the 6 major tidal components that contain more than 99.5% of the energy. The observed and simulated currents are in good agreement (Table 1), with bias and root mean square error (RMSE) in the tidal constituents (L_{maj} and L_{maj} together) were <1 cm/s and 2 cm/s, respectively. The observed and simulated orientation angles have negligible bias and RMSE of 4°. The bias and RMSE in the phases of the tidal constituents are 19° and 26°, respectively. Overall, the model reproduced the tidal constituents reasonably well.

3.3. Seasonal circulation patterns in Qatar EEZ

The seasonal circulation patterns, representing winter (January 2019), spring (April 2019), summer (July 2019) and autumn (October 2019), have been simulated, and the corresponding monthly-averaged currents are presented in Fig. 5. In January, the Iranian Coastal Current (ICC) flows towards northwest, while counterclockwise eddies with varying radii are formed in the deeper regions off Iran. Interestingly, a few counterclockwise eddies are formed in the offshore of northern Qatar and north of Bahrain and clockwise eddies in the south of Bahrain and in the Gulf of Salwa (GoS, Fig. 1). The four eddies in the GoS are peculiar not only by their clockwise path but co-occurred in a consecutive series within the limited area available. In April, the ICC also flows northwestward but the pattern of eddies in the deeper regions of the EEZ of Iran has been slightly modified compared to January. The number of small-scale eddies in the offshore regions

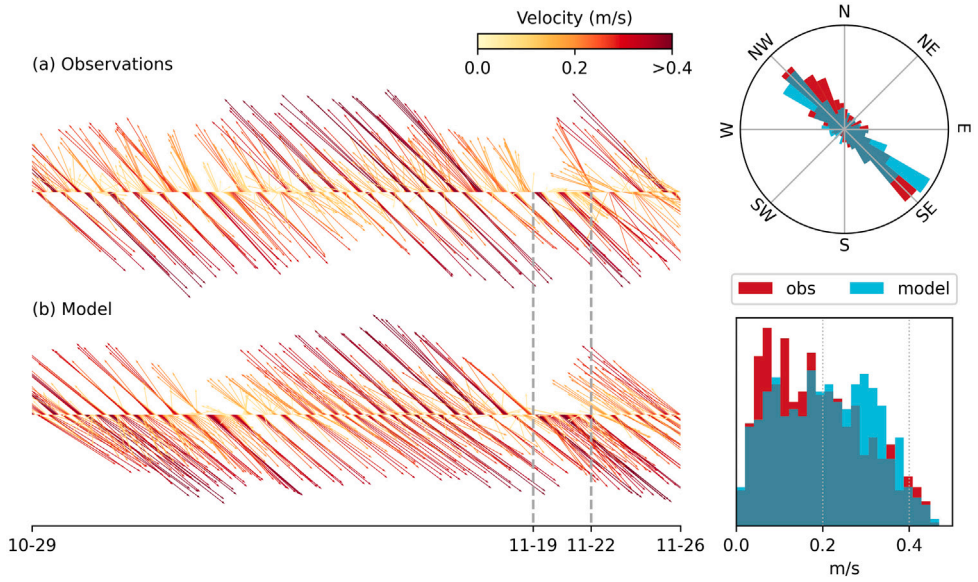

Fig. 3. Comparison between the (a) observed and (b) modelled hourly currents during 29 Oct–26 Nov, 2019 off Fuwairit, and histograms with the hourly current direction and amplitude. The model correctly reproduces both the current speed and direction. Strong Shamal winds prevented northwest currents during 19–22 Nov.

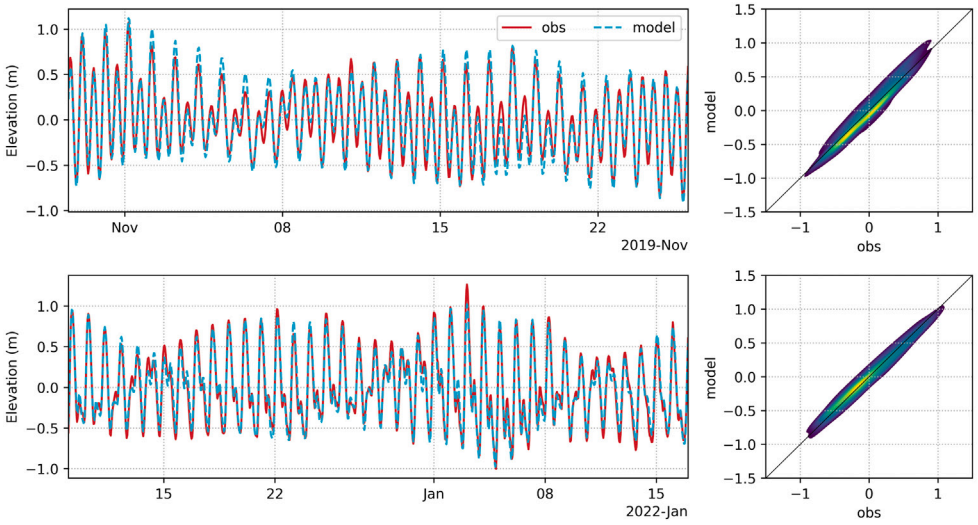

Fig. 4. Comparison between the observed and modelled SSE off Fuwairit (29 Oct–26 Nov, 2019, top) and in Doha Bay (08 Dec 2021–17 Jan 2022, bottom). In both cases, the model correctly reproduces the tidal cycle with a RMSE of less than 10 cm.

of northern Qatar has increased, while the eddies in the GoS have weakened. In July, the current speeds in the Gulf were relatively stronger, and we find two strong eddies near the Iranian coast — an anticlockwise eddy in the deep water and a clockwise eddy in the shallow water. Although this deep water eddy was already present in April, its strength has increased. At the same time, the eddies in the EEZ of Qatar have weakened, while the eddies in the GoS have strengthened. In October, the eddies gained more kinetic energy but the strength of northwest-flowing ICC also diminished. The central Gulf is then dominated by a few clockwise and counterclockwise eddies. The eddy in the south of Bahrain is intensified during this month, while the eddies in the GoS have weakened.

3.4. Flow around coastal structures

By using a very fine mesh resolution around artificial structures, the model can reproduce the fine-scale details of the flow around coastal structures. We analysed the maximum current speeds around the ports of Mesaieed, Ras Laffan and Al Ruwais, as well as along Doha's waterfront (Fig. 6). This analysis was performed from October 15th to November 30th 2019. Since the flow is mostly tidally driven, the maximum current speed patterns are similar to other periods of the year. Artificial structures can significantly intensify the current speed, especially around the corners of the structure and through narrow passages such as between breakwaters. Here, the current speeds at the edges and openings of the port of Ras Laffan structures are significantly high, exceeding 1 m/s. Similar magnitudes are found in the narrow channels and narrow openings in the Pearl Qatar, at the entry of the industrial port of Mesaieed and between the breakwaters of the port of Al Ruwais. By concentrating the flow energy through narrow passages, these structures not only locally intensify the circulation, but also hinder it just nearby where they provide sheltering. They therefore tend to increase the spatial variability of the current speed in their vicinity.

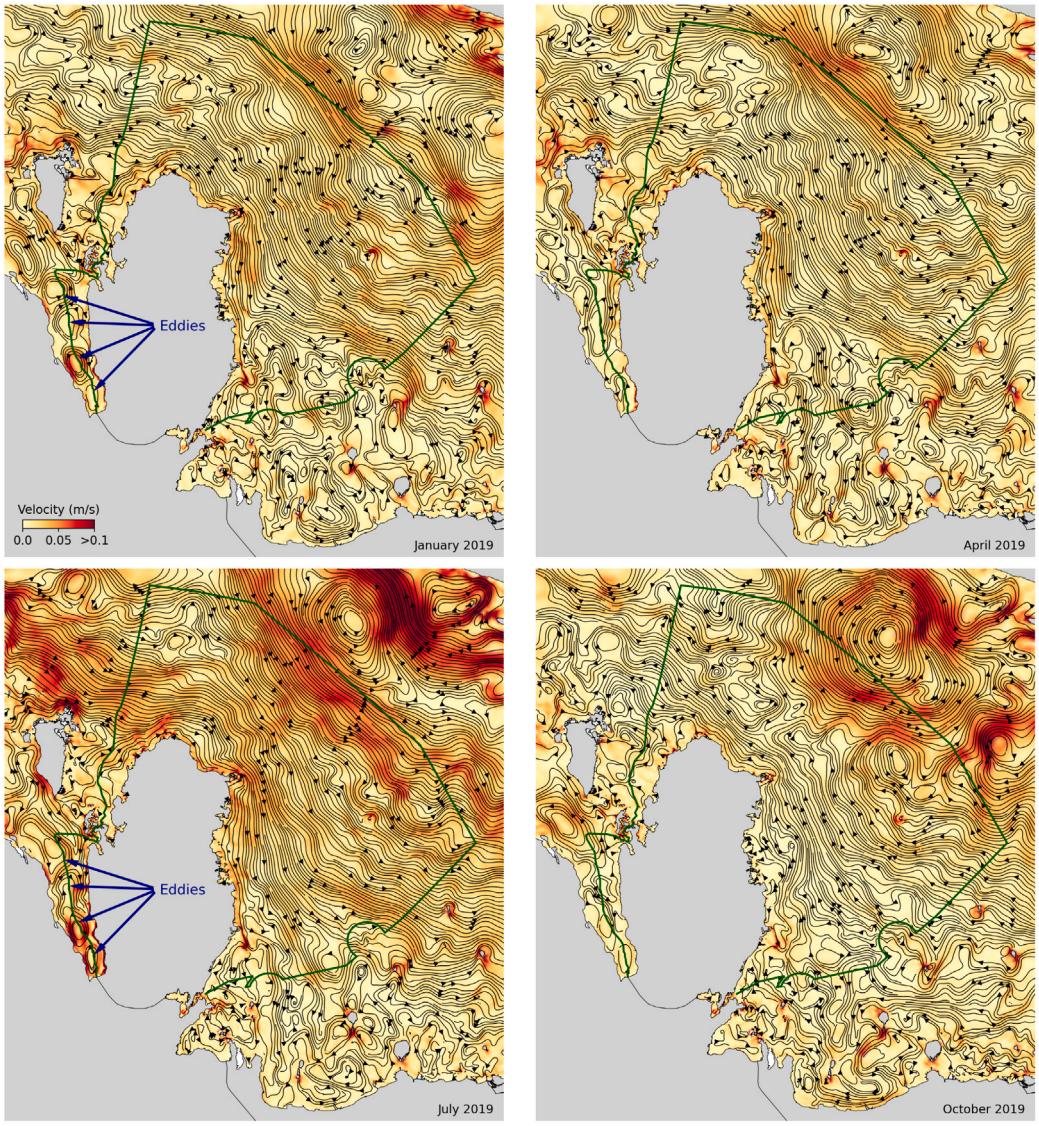

Fig. 5. Monthly-averaged circulation patterns in Qatar EEZ in January, April, July and October 2019. The colorbar is the same for all figures.

4. Discussion and conclusions

We have developed a multiscale hydrodynamic model of the entire Arabian/Persian Gulf with a particular focus on its central part. By using an unstructured mesh that allows local mesh refinements in topographically-challenging areas, the model can bridge the gap between the regional ($\gtrsim$100 km) and the structure scales ($\lesssim$100 m). This depth-averaged model was forced with ERA5 winds, the density field from an external baroclinic model, and the external circulation combined with the tidal forcing on the open boundary, in the Sea of Oman. The model results have been verified against current velocity and SSE observations at two different locations. We used the model to analyse the seasonality of the large-scale circulation, as well as the small-scale details of the flow around structures along the coast of Qatar. That allowed us to identify the peculiar eddy dynamics of the GoS, South of Bahrain. The derivation of the underlying mechanisms of eddy creation and decay remains quite elusive in the absence of accurate field measurements in that region. When simulating the flow dynamics around artificial structures, we could highlight how these structures modify the flow by locally intensifying it to current speeds beyond 1 m/s, while also hindering it just nearby. These structures therefore tend to greatly increase the spatial variability of the coastal ocean circulation.

The simulated regional circulation patterns and their seasonality are consistent with earlier studies of Reynolds (1993), Thoppil and Hogan (2010) and Pous et al. (2015). Our model results suggest that these patterns are accompanied by an intense eddy activity, which will influence the transport of tracers such as pollutants and biological material throughout the entire Gulf. In general, there are distinct circulation patterns in the central part of the Gulf, which are induced by winds, density gradients and bathymetry. Along the west/north and east offshore regions of Qatar EEZ, the resultant flow is towards the SE and S, respectively. This will enable the transport of particles or pollutants towards the respective coasts. Earlier studies reported that the net SE currents along with the NW winds in the northern Gulf cause transport and settling of marine litter (Veerasingam et al., 2020a), floating marine debris (Al-Khayat et al., 2021) and tarmat Veerasingam et al. (2020b) along the west coast of Qatar. The entrapped microplastics of Ras Rakan Island, on the northern coast of Qatar, was mainly transported by these flow characteristics (Veerasingam et al., 2021). The fine resolution model implemented in Qatar EEZ and the coastal eddies thus identified for the first time in this region indicate that a fine scale treatment of the fate and transport of the particles can be deemed through multiscale modelling.

By using a fine mesh resolution in the GoS, our study suggests the existence of a peculiar eddy dynamics in this enclosed water body. The

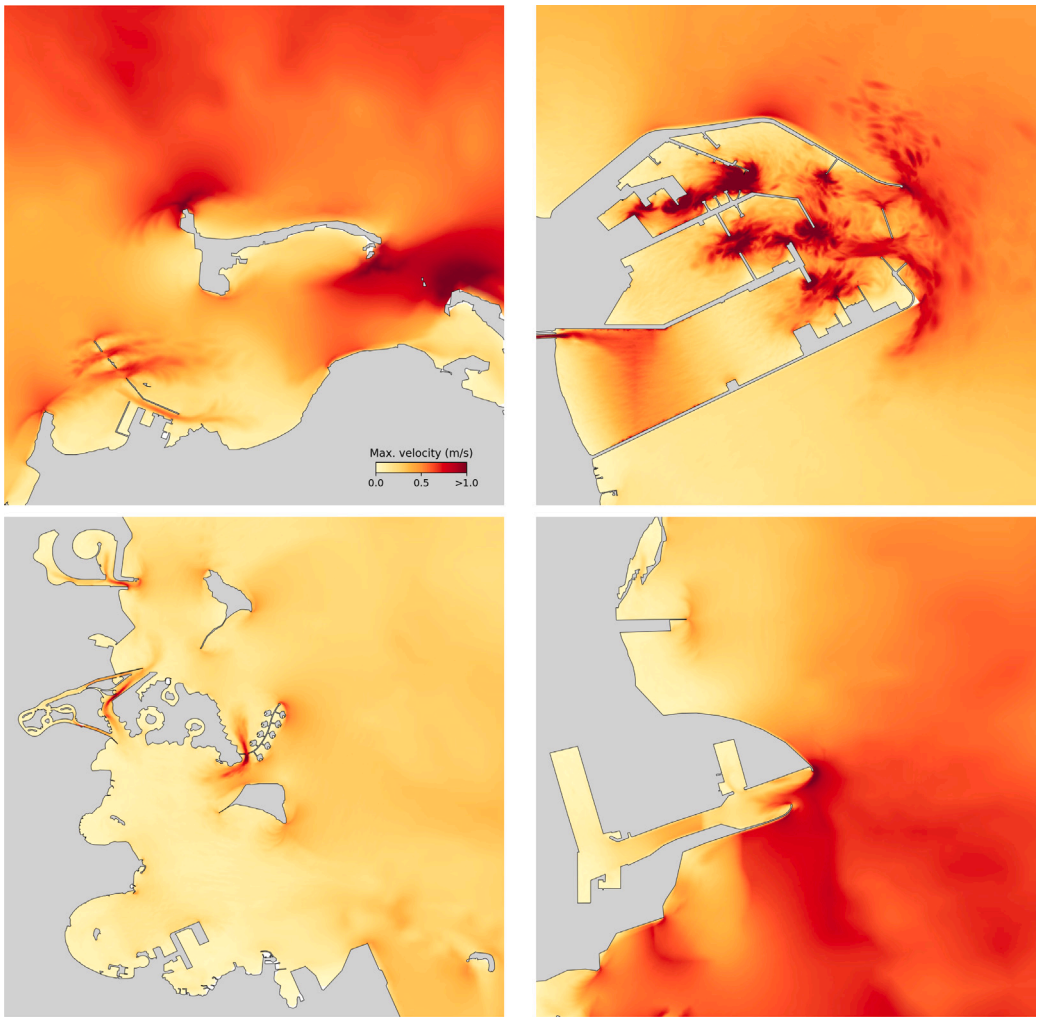

Fig. 6. Maximum current speed during Oct. 15–Nov. 30, 2019 near the four artificial structures highlighted in Fig. 2. The interaction of tidal currents with small-scale artificial structures can produce local currents above 1 m/s. The colorbar is the same for all figures.

co-occurrence of several eddies in a rather narrow area will reduce the water exchanges between the GoS and the rest of the Gulf. These exchanges are further reduced by the presence of coral reefs and a shallow seabed at the entry of the GoS. They could hence explain the large salinity, of the order of 60, observed in the GoS (Joydas et al., 2015). The four prominent eddies identified during winter decayed during spring, re-built during early summer and partially decayed during autumn. This has certain links with the Shamal winds as they are relatively strong during winter and early summer and weak during spring and autumn (Aboobacker et al., 2021b). However, derivation of the underlying mechanisms for the formation and decay of these eddies may be quite complicate, in the absence of accurate measurements in this region. It is inferred from literature that the salinity in the GoS is much higher compared to the adjacent regions. Thus, the stratification and destratification features in the GoS and their links with the formation of eddies are not well understood.

At the local scale, the model is able to highlight and quantify the modifications of the currents in the vicinity of man-made coastal structures. These modifications are symptomatic of ocean sprawl, which impacts marine ecosystems not only at the sites of construction but also produces larger-scale impacts through the alteration of the coastal circulation. To precisely quantify these impacts, it is therefore important to be seamlessly simulate the interplay between the regional and local circulations. Changes in the ocean currents directly impact the transport of sediments, dissolved pollutants, plastics and biological species such as coral larvae and turtle hatchlings. In particular, the nesting beaches of the endangered hawksbill turtle are located between the ports of Ras Laffan and Al Ruwais (Pilcher et al., 2015). The proposed multi-scale ocean modelling system would allow a precise quantification of impacts across a broad range of scales, and hence provide a better picture of the entire environmental footprint of artificial coastal structures.

We have considered a 2D model rather than a full 3D model to achieve higher spatial resolution and hence explicitly resolve small-scale topographical features. A 3D baroclinic model would have provided a better representation of the physical processes driving the ocean dynamics. However, using a 3D model would have also diverted the computational resources to resolving multiple vertical layers at the expense of the horizontal resolution required to simulate the flow around coastal structures. While our 2D model includes an horizontal baroclinic gradient, it remains quite approximative as the underlying the density field is computed on a rather coarse $1/12^\circ$ grid rather than on the fine model mesh. Density variations at a scale smaller than about 10 km are thus not taken into account. Finally, while the model achieves a very high spatial resolution, it is forced by a global atmospheric model with a 31 km resolution. Such a model does not precisely represent small-scale atmospheric processes like the land and sea breezes. A better representation of the coastal circulation would therefore be achieved by coupling our ocean model with a regional atmospheric model specifically parametrized for the Gulf area with a kilometre-scale resolution.

With the continued population growth along the coasts, artificial structures and land reclamation will keep on expanding. The Gulf has probably experienced one of the most rapid coastal development in the World. These changes have profoundly modified the coastal environment and the coastal circulation patterns. Our model can precisely represent these effects while, at the same time, also representing the large-scale circulation in the entire region. It paves the way for a better representation of transport processes in coastal environments dominated by artificial structures, and hence a better understanding of the local and non-local consequences of ocean sprawl. This has implications for sediment transport and coastal erosion, dispersal of biological organisms such as turtle hatchlings, jellyfishes, coral larvae, seagrass propagules and mangrove seeds, and the transport of pollutants such as oil spills and plastics.

CRediT authorship contribution statement

Emmanuel Hanert: Writing – review & editing, Writing – original draft, Visualization, Validation, Methodology, Investigation, Formal analysis, Data curation, Conceptualization. **Aboobacker Valliyil Mohammed:** Writing – original draft, Data curation. **Subramanian Veerasingam:** Data curation. **Thomas Dobbelaere:** Visualization, Software. **Valentin Vallaeys:** Visualization, Software. **Ponnumony Vethamony:** Writing – original draft, Conceptualization.

Declaration of competing interest

The authors declare the following financial interests/personal relationships which may be considered as potential competing interests: Emmanuel Hanert reports financial support, administrative support, and travel were provided by Catholic University of Louvain Earth and Life Institute.

Data availability

The computer code is freely available on a public git repository. The in situ data collected to validate the model can however not be shared.

Acknowledgements

We are grateful to Dr. Antoine Saint-Amand and Ms. Lauranne Alaerts for their help in producing some of the figures. We further thank Prof. Hamad Al-Saad Al-Kuwari, Director, Environmental Science Center (ESC), Qatar University (QU) for his constant encouragement and support. This work was jointly carried out by QU and UCLouvain under the QU Collaborative Grant project (QUCG-ESC-22/23-591), funded by QU, Qatar. Computational resources were provided by the Consortium des Équipements de Calcul Intensif (CÉCI), funded by the F.R.S.-FNRS, Belgium under Grant No. 2.5020.11.

References

Aboobacker, V.M., Samiksha, S.V., Veerasingam, S., Al-Ansari, E.M.A.S., Vethamony, P., 2021a. Role of shamal and easterly winds on the wave characteristics off Qatar, central Arabian Gulf. Ocean Eng. 236, 109457.

Aboobacker, V.M., Shanas, P.R., Al-Ansari, E.M.A.S., Kumar, V.S., Vethamony, P., 2021b. The maxima in northerly wind speeds and wave heights over the Arabian sea, the Arabian/Persian Gulf and the red sea derived from 40 years of ERA5 data. Clim. Dynam. 56, 1037–1052.

Aboobacker, V.M., Shanas, P.R., Veerasingam, S., Al-Ansari, E.M.A.S., Sadooni, F.N., Vethamony, P., 2021c. Long-term assessment of onshore and offshore wind energy potentials of Qatar. Energies 14 (1178).

Al-Ansari, E.M.A.S., Rowe, G., Abdel-Moati, M., Yigiterhan, O., Al-Maslamani, I., Al-Yafei, M., Al-Shaikh, I., Upstill-Goddard, R., 2015. Hypoxia in the central Arabian Gulf exclusive economic zone (EEZ) of Qatar during summer season. Estuar. Coast. Shelf Sci. 159, 60–68.

Al Azhar, M., Temimi, M., Zhao, J., Ghedira, H., 2016. Modeling of circulation in the Arabian Gulf and the sea of Oman: Skill assessment and seasonal thermohaline structure. J. Geophys. Res.: Oceans 121, 1700–1720.

Al-Khayat, J.A., Veerasingam, S., Aboobacker, V.M., Vethamony, P., 2021. Hitchhiking of encrusting organisms on floating marine debris along the west coast of Qatar, Arabian/Persian Gulf. Sci. Total Environ. 776, 145985.

Al Senafi, F., Anis, A., 2015. Shamals and climate variability in the northern Arabian/Persian Gulf from 1973 to 2012. Int. J. Climatol. 35, 4509–4528.

Al Senafi, F., Anis, A., 2020. Wind-driven flow dynamics off the northwestern Arabian Gulf coast. Estuar. Coast. Shelf Sci. 233, 106511.

Alosairi, Y., Pokavanich, T., 2017. Seasonal circulation assessments of the northern Arabian/Persian Gulf. Mar. Pollut. Bull. 116, 270–290.

Barth, H.J., Khan, N.Y., 2008. Biogeophysical setting of the Gulf. In: Protecting the Gulf's Marine Ecosystems from Pollution. Springer, pp. 1–21.

Becker, J., Sandwell, D., Smith, W., Braud, J., Binder, B., Depner, J., Fabre, D., Factor, J., Ingalls, S., Kim, S., et al., 2009. Global bathymetry and elevation data at 30 arc seconds resolution: SRTM30_PLUS. Mar. Geodesy 32, 355–371.

Belmonte Rivas, M., Stoffelen, A., 2019. Characterizing ERA-interim and ERA5 surface wind biases using ASCAT. Ocean Sci. 15, 831–852.

Belthaji, A., 1983. Some Oceanographic Measurements in the Gulf Waters Around Qatar Peninsula. Technical Report., Qatar University.

Bishop, M.J., Mayer-Pinto, M., Airoldi, L., Firth, L.B., Morris, R.L., Loke, L.H., Hawkins, S.J., Naylor, L.A., Coleman, R.A., Chee, S.Y., et al., 2017. Effects of ocean sprawl on ecological connectivity: Impacts and solutions. J. Exp. Mar. Biol. Ecol. 492, 7–30.

Blayo, E., Debreu, L., 2005. Revisiting open boundary conditions from the point of view of characteristic variables. Ocean Model. 9, 231–252.

de Brye, B., Shellen, S., Sassi, M., Vermeulen, B., Karna, T., Deleersnijder, E., 2011. Preliminary results of a finite-element, multi-scale model of the Mahakam delta (Indonesia). Ocean Dyn. 61, 1107–1120.

Burt, J.A., 2014. The environmental costs of coastal urbanization in the Arabian Gulf. City 18, 760–770.

Butler, J.D., Purkis, S.J., Yousif, R., Al-Shaikh, I., Warren, C., 2020. A high-resolution remotely sensed benthic habitat map of the qatari coastal zone. Mar. Pollut. Bull. 160, 111634.

Chao, S.Y., Kao, T.W., Al-Hajri, K.R., 1992. A numerical investigation of circulation in the Arabian Gulf. J. Geophys. Res.: Oceans 97, 11219–11236.

Codiga, D.L., 2011. Unified Tidal Analysis and Prediction using the UTide Matlab Functions. Technical Report 2011-01., Graduate School of Oceanography, University of Rhode Island.

Cushman-Roisin, B., Beckers, J.M., 2011. Introduction to Geophysical Fluid Dynamics. Elsevier.

Dobbelaere, T., Muller, E.M., Gramer, L.J., Holstein, D.M., Hanert, E., 2020. Coupled epidemio-hydrodynamic modeling to understand the spread of a deadly coral disease in Florida. Front Mar. Sci. 7 (1016).

Eager, R.E., Raman, S., Wootten, A., Westphal, D.L., Reid, J.S., A. Mandoos, A., 2008. A climatological study of the sea and land breezes in the Arabian Gulf region. J. Geophys. Res.: Atmos. 113.

Egbert, D., G, Erofeeva, S.Y., 2002. Efficient inverse modeling of Barotropic ocean tides. J. Atmos. Ocean. Technol. 19, 183–204.

Elobaid, E.A., Al-Ansari, E.M.A.S., Yigiterhan, O., Aboobacker, V.M., Vethamony, P., 2021. Spatial variability of summer hydrography in the central Arabian Gulf. Oceanologia http://dx.doi.org/10.1016/j.oceano.2021.09.003.

Ferry, N., Rémy, E., Brasseur, P., Maes, C., 2007. The Mercator global ocean operational analysis system: Assessment and validation of an 11-year reanalysis. J. Mar. Syst. 65, 540–560.

Firth, L.B., Knights, A.M., Bridger, D., Evans, A., Mieskowska, N., Moore, P.J., O'Connor, N.E., Sheehan, E.V., Thompson, R.C., Hawkins, S.J., 2016. Ocean Sprawl: Challenges and opportunities for biodiversity management in a changing world. Oceanogr. Mar. Biol. Ann. Rev. 54, 193–269.

Frys, C., Saint-Amand, A., Le Hénaff, M., Figueiredo, J., Kuba, A., Walker, B., Lambrechts, J., Vallaeys, V., Vincent, D., Hanert, E., 2020. Fine-scale coral connectivity pathways in the Florida reef tract: Implications for conservation and restoration. Front. Mar. Sci. 7 (312).

Geuzaine, C., Remacle, J.F., 2009. Gmsh: A 3-D finite element mesh generator with built-in pre- and post-processing facilities. Internat. J. Numer. Methods Engrg. 156 (6), 1297–1309.

Heery, E.C., Bishop, M.J., Critchley, L.P., Bugnot, A.B., Airoldi, L., Mayer-Pinto, M., Sheehan, E.V., Coleman, R.A., Loke, L.H., Johnston, E.L., et al., 2017. Identifying the consequences of ocean sprawl for sedimentary habitats. J. Exp. Mar. Biol. Ecol. 492, 31–48.

Hosseinibalam, F., Hassanzadeh, S., Rezaei-Latifi, A., 2011. Three-dimensional numerical modeling of thermohaline and wind-driven circulations in the Persian Gulf. Appl. Math. Model. 35, 5884–5902.

Hunter, J., 1982. The physical oceanography of the Arabian Gulf:A review and theoretical interpretation of previous observations. In: The First Arabian Gulf Conference on Environment and Pollution. Kuwait University, Faculty of Science, Kuwait, pp. 1–23.

Hunter, J., 1983. Aspects of the dynamics of the residual circulation of the Arabian Gulf. In: Coastal Oceanography. Springer, pp. 31–42.

J., Kämpf, Sadrinasab, M., 2005. The circulation of the Persian Gulf: A numerical study. Ocean Sci. 2, 27–41.

Johns, W.E., Yao, F., Olson, D., Josey, S., Grist, J., Smeed, D., 2003. Observations of seasonal exchange through the straits of Hormuz and the inferred heat and freshwater budgets of the Persian Gulf. J. Geophys. Res.: Oceans 108.

Joydas, T., Qurban, M.A., Manikandan, K., Ashraf, T., Ali, S., Al-Abdulkader, K., Qasem, A., Krishnakumar, P., 2015. Status of macrobenthic communities in the hypersaline waters of the Gulf of Salwa, Arabian Gulf. J. Sea Res. 99, 34–46.

Khan, N.Y., Munawar, M., Price, A.R., 2002. The Gulf Ecosystem: Health and Sustainability. Backhuys Leiden, The Netherlands.

Lambrechts, J., Hanert, E., Deleersnijder, E., Bernard, P.E., Legat, V., Remacle, J.F., Wolanski, E., 2008. A multi-scale model of the hydrodynamics of the whole great barrier reef. Estuar. Coast. Shelf Sci. 79, 143–151.

Le Bars, Y., Vallaeys, V., Deleersnijder, É., Hanert, E., Carrere, L., Channelière, C., 2016. Unstructured-mesh modeling of the Congo river-to-sea continuum. Ocean Dyn. 66, 589–603.

Legrand, S., Deleersnijder, E., Hanert, E., Legat, V., Wolanski, E., 2006. High-resolution, unstructured meshes for hydrodynamic models of the great barrier reef, Australia. Estuar. Coast. Shelf Sci. 68, 36–46.

Lentz, S.J., Davis, K.A., Churchill, J.H., DeCarlo, T.M., 2017. Coral reef drag coefficients–water depth dependence. J. Phys. Oceanogr. 47, 1061–1075.

Mahmoodi, K., Ghassemi, H., Razminia, A., 2019. Temporal and spatial characteristics of wave energy in the Persian Gulf based on the ERA5 reanalysis dataset. Energy 187, 115991.

Martín-Antón, M., Negro, V., del Campo, J.M., López-Gutiérrez, J.S., Esteban, M.D., 2016. Review of coastal land reclamation situation in the world. J. Coast. Res. 66, 7–671.

Monismith, S.G., 2007. Hydrodynamics of coral reefs. Annu. Rev. Fluid Mech. 39 (1), 37–55.

Pilcher, N.J., Al-Maslamani, I., Williams, J., Gasang, R., Chikhi, A., 2015. Population structure of marine turtles in coastal waters of Qatar. Endanger. Species Res. 28, 163–174.

Pous, S., Lazure, P., Carton, X., 2015. A model of the general circulation in the Persian Gulf and in the strait of Hormuz: Intraseasonal to interannual variability. Cont. Shelf Res. 94, 55–70.

Price, A., Sheppard, C., Roberts, C., 1993. The Gulf: its biological setting. Mar. Pollut. Bull. 27, 9–15.

Rakib, F., Al-Ansari, E.M.A.S., Husrevoglu, Y.S., Yigiterhan, O., Al-Maslamani, I., Aboobacker, V.M., Vethamony, P., 2021. Observed variability in physical and biogeochemical parameters in the central Arabian Gulf. Oceanologia 63, 227–237.

Rao, P.G., Hatwar, H., Al-Sulaiti, M.H., Al-Mulla, A.H., 2003. Summer shamals over the Arabian Gulf. Weather 58, 471–478.

Reynolds, R.M., 1993. Physical oceanography of the Persian Gulf, strait of Hormuz, and the Gulf of Oman - results from the Mt. Mitchell expedition. Mar. Pollut. Bull. 27, 35–59.

Riegl, B.M., Purkis, S.J., 2012. Coral reefs of the Gulf: Adaptation to climatic extremes in the world's hottest sea. In: Coral Reefs of the Gulf. Springer, pp. 1–4.

Sandeepan, B., Panchang, V.G., Nayak, S., Kumar, K.K., Kaihatu, J.M., 2018. Performance of the WRF model for surface wind prediction around Qatar. J. Atmos. Ocean. Technol. 35, 575–592.

Sheppard, C., Al-Husiani, M., Al-Jamali, F., Al-Yamani, F., Baldwin, R., Bishop, J., Benzoni, F., Dutrieux, E., Dulvy, N.K., Durvasula, S.R.V., et al., 2010. The Gulf: A young sea in decline. Mar. Pollut. Bull. 60, 13–38.

Smagorinsky, J., 1963. General circulation experiments with the primitive equations. Mon. Weather Rev. 91, 99–164.

Smith, S., Banke, E., 1975. Variation of the sea surface drag coefficient with wind speed. Q. J. R. Meteorol. Soc. 101, 665–673.

Swift, S.A., Bower, A.S., 2003. Formation and circulation of dense water in the Persian/Arabian Gulf. J. Geophys. Res.: Oceans 108 (C1), 3004.

Thomas, C.J., Lambrechts, J., Wolanski, E., Traag, V.A., Blondel, V.D., Deleersnijder, E., Hanert, E., 2014. Numerical modelling and graph theory tools to study ecological connectivity in the great barrier reef. Ecol. Model. 272, 160–174.

Thoppil, P.G., Hogan, P.J., 2010. A modeling study of circulation and eddies in the Persian Gulf. J. Phys. Oceanogr. 40, 2122–2134.

UNEP-WCMC, 2021. Global Distribution of Warm-Water Coral Reefs, Compiled from Multiple Sources Including the Millennium Coral Reef Mapping Project. Technical Report Version 4.1., WorldFish Centre, WRI, TNC, http://dx.doi.org/10.34892/t2wk-5t34.

Vallaeys, V., Lambrechts, J., Delandmeter, P., Pätsch, J., Spitzy, A., Hanert, E., Deleersnijder, E., 2021. Understanding the circulation in the deep, micro-tidal and strongly stratified Congo river estuary. Ocean Model. 167, 101890.

Veerasingam, S., Al-Khayat, J.A., Aboobacker, V.M., Hamza, S., Vethamony, P., 2020a. Sources, spatial distribution and characteristics of marine litter along the west coast of Qatar. Mar. Pollut. Bull. 159, 111478.

Veerasingam, S., Al-Khayat, J.A., Haseeba, K.P., Aboobacker, V.M., Hamza, S., Vethamony, P., 2020b. Spatial distribution, structural characterization and weathering of tarmats along the west coast of Qatar. Mar. Pollut. Bull. 159, 111486.

Veerasingam, S., Vethamony, P., Aboobacker, V.M., Giraldes, A.E., Dib, S., Al-Khayat, J.A., 2021. Factors influencing the vertical distribution of microplastics in the beach sediments around the Ras Rakan Island, Qatar. Environ. Sci. Pollut. Res. 1–10.

Vethamony, P., Reddy, G., Babu, M., Desa, E., Sudheesh, K., 2005. Tidal eddies in a semi-enclosed basin: A model study. Mar. Environ. Res. 59, 519–532.

Victoria, I., 2011. Measuring currents in demanding environments with a Seaguard®RCM. In: 2011 IEEE/OES 10th Current, Waves and Turbulence Measurements. CWTM, IEEE, pp. 237–245.

Yousif, R.A., 2016. Hydrodynamic modelling of the northeastern Qatar coast for assessment of sensitive ecosystems under anthropogenic and natural stressors. In: Qatar Foundation Annual Research Conference Proceedings Volume 2016 Issue 1. Hamad bin Khalifa University Press (HBKU Press), p. EEPP1918.

Yousif, R., Warren, C., Ben-Hamadou, R., Husrevoglu, S., 2018. Modeling sediment transport in Qatar: Application for coastal development planning. Integr. Environ. Assess. Manag. 14, 240–251.

Yu, Y., Notaro, M., Kalashnikova, O.V., Garay, M.J., 2016. Climatology of summer Shamal wind in the middle east. J. Geophys. Res.: Atmos. 121, 289–305.